Published in final edited form as:

J Am Chem Soc. 2019 July 17; 141(28): 11009–11018. doi:10.1021/jacs.8b13493.

A Responsive Magnetic Resonance Imaging Contrast Agent for Detection of Excess Copper(II) in the Liver *In Vivo*

Namini N. Paranawithana[†], **Andre F. Martins**[†,§], **Veronica Clavijo Jordan**[‡,#], **Piyu Zhao**[†], **Sara Chirayil**[‡], **Gabriele Meloni**[†], **A. Dean Sherry**[*,†,‡]

[†]Department of Chemistry and Biochemistry, University of Texas at Dallas, Richardson, Texas, United States

[‡]Advanced Imaging Research Center, University of Texas Southwestern Medical Center, Dallas, Texas, United States

Abstract

The design, synthesis, and properties of a new gadolinium-based copper-responsive magnetic resonance imaging (MRI) contrast agent is presented. The sensor (GdL_1) has high selectivity for copper ions and exhibits a 43% increase in r_1 relaxivity (20 MHz) upon binding to 1 equiv of Cu^{2+} in aqueous buffer. Interestingly, in the presence of physiological levels of human serum albumin (HSA), the r_1 relaxivity is amplified further up to 270%. Additional spectroscopic and X-ray absorption spectroscopy (XAS) studies show that Cu^{2+} is coordinated by two carboxylic acid groups and the single amine group on an appended side chain of GdL_1 and forms a ternary complex with HSA (GdL_1–Cu^{2+}–HSA). T_1-weighted *in vivo* imaging demonstrates that GdL_1 can detect basal, endogenous labile copper(II) ions in living mice. This offers a unique opportunity to explore the role of copper ions in the development and progression of neurological diseases such as Wilson's disease.

Graphical Abstract

[*]**Corresponding Author**: dean.sherry@utsouthwestern.edu; sherry@utdallas.edu.
[§]Werner Siemens Imaging Center, University Hospital Tuebingen (UKT), Roentgenweg 13, 72076 Tübingen, German.
[#]Athinoula A. Martinos Centre for Biomedical Imaging, Massachusetts General Hospital, Harvard Medical School, Charlestown, Massachusetts, 02129, United States.

The authors declare no competing financial interest.

ASSOCIATED CONTENT

Supporting Information

The Supporting Information is available free of charge on the ACS Publications website at DOI: 10.1021/jacs.8b13493.

Synthesis details for preparing the Gd complexes, experimental details of the relaxometric experiments, titrations, ^{17}O NMR experiments, EPR spectra, EXAFS spectra, cyclic voltammetry, computational model details, and MR images (PDF)

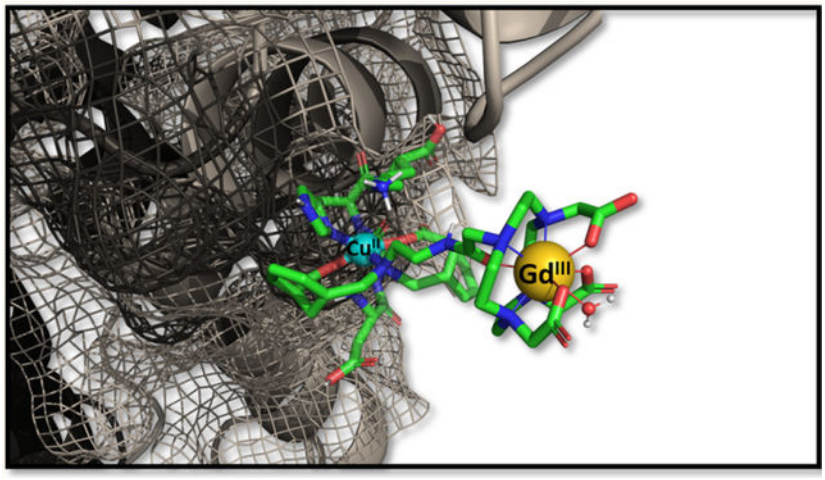

1. INTRODUCTION

Copper is the third most abundant transition metal in the body and a required dietary nutrient. The average healthy human has a total of ~110 mg of copper in tissues.[1–4] Copper is typically bound to specific proteins and enzymes where it plays fundamental catalytic and structural roles.[5–7] Copper has also been associated with signaling events in the brain.[8–10] In a biological environment, copper is present in two oxidation states, the cuprous (Cu^{+}) and cupric (Cu^{2+}) ions.[11] Typically, total extracellular Cu^{2+} can vary widely from nM to μM, while intracellular Cu^{+} can vary from μM to mM.[12–14] Due to its redox properties, copper homeostasis is tightly regulated in cells and disruption of this is associated with a number of neurodegenerative diseases including Alzheimer's, Parkinson's, prion, familial amyotrophic lateral sclerosis, Menkes and Wilson's diseases.[15–18] For instance, genetic mutations of copper-transporting proteins ATP7A and ATP7B result in afflictions of systemic brain copper deficiency in Menkes disease and hyperaccumulation of hepatic copper ions in Wilson's disease, respectively.[19–22] Accumulation of copper in the liver of Wilson's disease patients ranges from a few micromolar to several millimolar.[23] Although copper ion homeostasis and the impact of abnormal copper levels on physiology have been widely studied, details about the functional role of copper ions in various tissues *in vivo* remain insufficiently understood due to lack of real-time copper imaging techniques in live animals.[24,25]

Magnetic resonance imaging (MRI) is a powerful medical diagnostic technique that allows noninvasive, three-dimensional visualization of tissue with high spatial and temporal resolution. MRI is largely based on detection of water and fat protons so that image contrast among tissues reflects differences in proton content, cell density, and water perfusion and diffusion. Image contrast can be altered by the use of paramagnetic inorganic complexes that shorten the $T_{1,2}$ relaxation times of water molecules in various compartments. These agents are commonly known as contrast agents (CAs). Among all paramagnetic complexes designed for use as CAs, the Gd^{3+}-based agents have proven to be the safest and most versatile agents for clinical use over the past ~30 years. The efficiency of an agent per unit concentration is commonly reported as r_1 (T_1) or r_2 (T_2) relaxivity.[26–28] Notably,

the design of contrast agents that alter the T_1 of water protons in response to a given analyte is of major importance. Many responsive probes have been reported including sensors for metal ions,[9] enzyme activity,[29] pH,[30] pO_2,[31] and temperature.[32] One of the first reports of a copper-activated MR sensor was based on a GdDO3A (1,4,7,10-tetraazacyclododecane-1,4,7,-triacetic acid) derivative having a iminodiacetate pendant arm for Cu^{2+} recognition. This derivative displayed a 41% increase in r_1 relaxivity upon binding Cu^{2+}.[33] A later paper reported a GdDO3A derivative having a quinolone-based pendant arm,[34] and it displayed a 71% increase in r_1 upon addition of Cu^{2+}. Neither of these agents were examined *in vivo*. Derivatives have also been designed to show greater selectivity for Cu^{+} over Cu^{2+}.[35] In addition to MRI agents, other imaging approaches for imaging copper have included positron emission tomography (PET), optical imaging, and bimodal imaging techniques.[36,37] The positron emitter, ^{64}Cu, was successfully used to image greater uptake and accumulation of copper in livers of Wilson's disease mouse models.[24] Similarly, a near-infrared fluorescent sensor for detection of Cu^{+} ions has been shown to be capable of monitoring fluctuations in exchangeable copper stores in living cells and mice under basal conditions, as well as in situations of copper overload or deficiency.[38]

Our group recently reported several MR zinc-sensors capable of detecting the release of intracellular stores of zinc into extracellular space in prostate[39] and pancreas of live mice.[40] Divalent zinc ions released by cells in these organs are immediately chelated by a zinc-responsive MR agent, and the resulting binary complex then forms a ternary complex with serum albumin which results in reduced molecular motion and an increase of r_1.[41,42] Copper is also known to bind to albumin and other less abundant proteins in plasma.[43–47] Hence, we hypothesized that the key to an effective copper detection *in vivo* by MRI might be to design a Cu-responsive agent that also forms a ternary complex between Cu^{2+} ions, the sensor, and albumin, similar to the Zn-sensor designs.

Herein, we report the synthesis of a novel copper-responsive MRI contrast agent having a bis(benzoic acid)methylamine recognition motif (GdL_1) and the physicochemical properties of the resulting GdL_1–Cu^{2+} complex and the ternary complex formed with human serum albumin (HSA). X-ray absorption spectroscopy (XAS) of GdL_1 and some structural analogues was used to interrogate the Cu^{2+} binding site in this system. Finally, GdL_1 was injected into mice to detect extracellular Cu^{2+} in the liver by MRI. A comparison of GdL_1 (high Cu^{2+} affinity) with GdL_2 and GdL_3 (lower Cu^{2+} affinity) (Figure 1) indicated that only GdL_1 detects extracellular copper in mouse liver.

2. RESULTS AND DISCUSSION

Design and Synthesis.

The structure of the Cu^{2+}-responsive agent reported here consists of a GdDO3A moiety with a bis(benzoic acid)methylamine side chain as a potential chelator for Cu^{2+}. This design was motivated by our previous MR-responsive Zn^{2+} sensor scaffold where the ion of interest initiates formation of a ternary complex between the agent and serum albumin.[41,42] Although Cu^{2+} has a preference for nitrogen donor atoms, the coordination rigidity provided by the bis(benzoic acid)methylamine could potentially favor coordination by geometrical stabilization of tetragonal or square pyramidal structures typical for Cu^{2+}.[48,49]

This structural feature precludes the possibility of binding with the more abundant biological ions like Ca^{2+} and Mg^{2+}. To evaluate the impact of repositioning of the carboxylate groups on the aromatic side chain and lowering the charge on the carboxylate groups, GdL_2 and GdL_3 were also studied for comparison. The synthetic details of all three contrast agents are described in the Supporting Information.

Water Proton Relaxivity Measurements in the Presence of Various Metal Ions.

The longitudinal relaxivity (r_1) of GdL_1 (4.7 ± 0.1 mM^{-1} s^{-1} at 20 MHz) was unchanged upon addition of Ca^{2+}, Mg^{2+}, Cu^{+}, or Fe^{3+} ions (Figure 2 and Figure S4). However, addition of Zn^{2+} increased r_1 to 5.3 mM^{-1} s^{-1} (a 12% increase), while addition of Cu^{2+} increased r_1 to 6.7 mM^{-1} s^{-1} (a 43% increase). The background relaxivity due to the weak paramagnetism of Cu^{2+} and Fe^{3+} was subtracted from the r_1 values shown in Figure 2 and reported in Table 1.[50] This suggests that GdL_1 has some selectivity for Cu^{2+} over Zn^{2+} in agreement with the Irving–William series and Pearson's hard–soft acid base (HSAB) theories.[51] Even though the origin of this r_1 enhancement is unclear from these data alone, one possibility is that the linker side arm with the anionic carboxyl groups on the bis-benzoic acid motif may form a hydrogen bond with the single exchanging inner-sphere water molecule on the Gd^{3+} ion and this interaction is reduced when Cu^{2+} or Zn^{2+} binds to GdL_1. This could in principle alter the water exchange rate in this system and result in a small change in r_1. A second contributing factor might be that GdL_1 experiences relatively slower molecular rotation (τ_R) upon binding to Cu^{2+}, and this could result in a slight increase in r_1 relaxivity. These two possibilities were examined in more detail below.

The binding stoichiometry between GdL_1 and Cu^{2+} was determined to be 1:1, as reported by the method of continuous variations (see the Job plot, Figure S9) and by an inflection point[52] in the relaxivity data (Figure 3). This stoichiometry was assumed in all calculations of dissociation constants (K_d). The increases in r_1 of GdL_2 and GdL_3 were considerably lower upon addition of Cu^{2+} (Figure 3), suggesting that either these two complexes have a weaker affinity for Cu^{2+} or the resulting GdL_x–Cu^{2+} complexes have quite different water exchange properties.

Binding Experiments in the Absence of HSA (GdL_x–Cu^{2+}).

The equilibrium dissociation constants (K_d) between the three GdL_x complexes and Cu^{2+} were determined by fluorescence spectroscopy by performing titrations in which Cu^{2+} was added to a buffered solution containing GdL_x. Addition of Cu^{2+} results in quenching of the intrinsic fluorescence of the benzoic acid moieties of GdL_x (Figure S11).[53,54] The resulting binding curves were fit to a 1:1 binding model to give the K_d values reported in Table 1. These data indicate that GdL_1 has the highest affinity for Cu^{2+} (84 ± 10 μM), followed by GdL_3 (352 ± 9 μM) and GdL_2 (895 ± 32 μM). This suggests that the position of the carboxyl groups (meta versus para) and charge of the complexes are both important for Cu^{2+} binding.

Water Proton Relaxivity Measurements in the Presence of Various Metal Ions and HSA.

HSA, the most abundant protein in serum (~600 μM), plays a key role in the transport of metal ions, fatty acids, and other hydrophobic molecules including many drugs. HSA has two Cu^{2+} binding sites, the N-terminal site (NTS) and the multimetal binding site

(MBS).[55,56] It was reported that Cu^{2+} has a significantly higher affinity for the NTS site (~1 pM)[57] than the MBS site (~10 nM).[58] Thus, the NTS site is considered to be the only site in HSA to be occupied by Cu^{2+}, since the concentration of HSA is much higher than the biological concentration of free Cu^{2+} ions.[55–59] We recently demonstrated that analogous Gd-based MR contrast agents responded to an increase in free Zn^{2+} ions from pancreatic β-cells[40] and epithelial prostate cells stimulated by an increase in plasma glucose.[39] This functional response was shown to reflect the formation of a ternary GdL_X–Zn-albumin complex at the MBS site A.[60] This previous data suggested that perhaps Cu^{2+} could also be detected *in vivo* in those situations where excess free Cu^{2+} ions in extracellular spaces might be available for binding to a contrast agent. This motivated further relaxometric studies to determine the magnetic contributions of all of the GdL_X with Cu^{2+} in the presence of physiological levels of HSA. As summarized in Table 1, the r_1 values for all three complexes increase slightly in the presence of HSA alone (likely reflecting a slight increase in viscosity) but increase substantially after the addition of Cu^{2+} ions. This suggests that the GdL_X complexes experience slower molecular rotation by the formation of a GdL_X–Cu–HSA ternary complex. This is particularly true for GdL_1 where r_1 increases from 6.1 ± 0.1 to 22.6 ± 0.2 mM^{-1} s^{-1} (a 270% increase). As shown in Figure 2 (and Figure S5), addition of Mg^{2+}, Ca^{2+}, and Fe^{3+} does not result in an increase in r_1 in the presence of HSA, while Zn^{2+} ions do to a lesser extent, about 2-fold lower than the increase in r_1 induced by Cu^{2+}.

Binding Experiments in the Presence of HSA.

Additional proton relaxation enhancement (PRE) titrations were carried out to examine the binding interactions and to quantitatively evaluate the binding constants for each GdL_X complex with HSA in the presence of 1 mol equiv of Cu^{2+}. A fitting of these data (Figure S13 and Table S2) to a 1:1 binding model gave the K_d values reported in Table 1. GdL_1 showed the highest binding affinity to HSA–Cu^{2+} (K_d = 45 ± 3.1 μM), while the binding affinities of GdL_2 and GdL_3 were surprisingly weaker only by ~30%. This demonstrates significant differences in binding affinity between the different GdL_X and Cu^{2+} are leveled upon formation of the ternary GdL_X–Cu^{2+}–HSA complexes. These data alone suggest that HSA plays a significant role in stabilizing the binding interactions between GdL_X and Cu^{2+} ions. To confirm the formation of the LnL_X–Cu^{2+}–HSA ternary complex, samples of LaL_1 (a diamagnetic analogue), Cu^{2+}, and HSA (from an EPR experiment, see below) were passed through a size exclusion chromatography column, and the eluent peaks were separately analyzed for Cu and La by ICP-MS. Those results (Figure S12 and Table S1) showed that ~63% of the total La eluted from the column in the form of a ternary LaL_1–Cu^{2+}–HSA complex, confirming the formation of a stable Cu^{2+} mediated ternary complex.

Kinetic Inertness.

The kinetic stability of a GdL_X complex is also an important factor to consider when developing MRI probes. Previous studies reported that Cu^{2+} could displace Gd^{3+} from a complex by transmetalation.[61,62] This possibility was examined by challenging GdL_1 with 3 mol equiv of Cu^{2+} in 0.03 M phosphate buffer (pH 7.2). Under these conditions, if transmetalation occurred, any unchelated Gd^{3+} would then precipitate from the solution as an insoluble phosphate, a process that can be monitored by relaxometry. R_{1obs} values measured over the time (Figure S16) show that complexes are kinetically inert, even in the

presence of a 3-fold excess of Cu^{2+}. In addition, LC-MS data showed that in the presence of a 1 mol equiv of Cu^{2+} no metal transmetalation was observed at room temperature after 7 days in MOPS buffer.

Experiments to Identify the Cu^{2+} Donor Atoms in GdL_1.

The X-band EPR spectrum of LaL_1–Cu^{2+} exhibited an unusual axial spectrum (devoid of well-defined hyperfine features and $g_\perp \cong 1.99$) both in the absence and in the presence of HSA (Figure S19). The $g_\perp$ values shown by these spectra significantly deviated from the typical values of an axial EPR spectrum for a type-2 Cu^{2+} complex. This suggests that the Cu^{2+} centers in both complexes are electron poor, likely due to the strong electron withdrawing effect of the lanthanum ion in the complex. In comparison, the X-band EPR spectrum of HSA–Cu^{2+} exhibited a typical type-2 square pyramidal geometry very similar to previously reported EPR spectra in the literature.[63] However, the broadened hyperfine features of the Cu^{2+} EPR spectra after addition of LaL_1 precluded a detailed structural analysis of the copper center.

XAS Studies.

Copper K-edge X-ray absorption spectroscopy (XAS) studies were also performed to identify the Cu^{2+} donor atoms in GdL_1–Cu^{2+} and GdL_1–Cu^{2+}–HSA. The XANES spectrum of GdL_1–Cu^{2+} (Figure 4) is characterized by an intense absorption feature at 8987–8988 eV with a broad low energy tail in the region below 8985 eV (normalized absorption of approximately 0.5 at 8988 eV) arising from a 1s → 4p transition characteristic of Cu^{2+} complexes. The presence of the first major inflection point at 8986 eV and the absence of lower energy features (normalized absorption 0.15 at 8984 eV and first inflection point 8984 eV) is typical of classic tetragonal Cu^{2+} complexes with nitrogen and oxygen ligands. The complex also presents a weak 8979 eV peak (more visible in the first derivative spectra) corresponding to the 1s → 3d transition possibly reflecting a less centrosymmetric nature of the center and thus a significant degree of distortion from planarity.[64] The XANES spectrum of GdL_1–Cu^{2+}–HSA is nearly identical to the spectrum of Cu^{2+}–HSA, suggesting a very similar coordination environment in the two complexes. The spectra are characterized by an intense absorption feature at 8987–8988 eV arising from a 1s → 4p transition. Additional features for the Cu^{2+} site include a lower-energy feature with normalized absorption of approximately 0.25 at 8984 eV and the first inflection point determined in the first derivative spectrum at 8982 eV, about ~1 eV higher than the one observed in Cu^{+} complexes. Possible photoreduction of Cu^{2+} was prevented experimentally by collecting the spectra at different locations in the frozen sample in each scan. Also, the XANES spectra were quite similar to the one observed for the Cu^{2+}–DAHK peptide complex representing the N-terminal Cu^{2+} binding site in HSA, thus supporting the same coordination environment as in the full-length protein.[55]

Additional information on coordination environment and ligand metal distances were obtained by copper K-edge extended X-ray absorption fine structure (EXAFS). The experimental copper EXAFS spectra are presented in Figure S20 together with best fits and the corresponding EXAFS Fourier transforms. The spectrum of GdL_1–Cu^{2+} could be fitted with two ligand shells indicative of a Cu complex coordinated by three N/O ligands at

1.99 Å and a N/O ligand at 2.51 Å (Table 2). The XANES and EXAFS results are consistent with the formation of a distorted tetragonal complex in which two O donor atoms from the two carboxylates plus one N atom from tertiary amine of the bis(benzoic acid)methylamine moiety and fourth donor O atom contributed by a solvent water molecule to the Cu^{2+} ion.

In the HSA-Cu^{2+} complex, the EXAFS data were best fit with three coordinating shells around Cu^{2+} with three Cu–O/N bonds at 1.99 Å and an additional (likely equatorial) N/O bond at 2.28 Å. In addition, a third shell corresponding to a N/O ligand at 2.51 Å was obtained in the fit, suggesting the presence of an axial ligand. This analysis was in agreement with a previously reported square pyramidal Cu^{2+}–HSA coordination at the N-terminal site (also known as ATCUN) with high affinity for Cu^{2+}.[55] Copper is coordinated to four nitrogen donors in the NTS site consisting of Asp, Ala, and His amide nitrogen atoms and the His side chain in an equatorial position and a water molecule or N-terminal amine nitrogen in the axial position.[55,59] For the GdL_1–Cu^{2+}–HSA ternary complex, the EXAFS data could be best fitted with three or four N/O ligands (resulting in similar F-values) at 1.96 Å and two additional N/O ligands at 2.33 and 2.86 Å. The analysis predicts the presence of a distorted square pyramidal/octahedral coordination around the Cu^{2+} in the ternary complex with four equatorial ligands with short bond distances and one or two axial ligands with longer bond distance (Table 2). This coordination anticipates the replacement of a loosely bound axial ligand in the Cu^{2+}–HSA complex by the chelating sites in the bis(benzoic acid)methylamine moiety of GdL_1. It should be noted that the bond distances for the distorted square pyramidal Cu^{2+}–HSA complex are distinctly different from the bond distances of the distorted square pyramidal ternary complex. Despite being difficult to unambiguously distinguish the coordination of one or two axial ligands by XAS, the EXAFS analysis confirms small differences in the coordination shells between GdL_1–Cu^{2+}–HSA and HSA–Cu^{2+}. This distorted octahedral or square pyramidal coordination of Cu^{2+} in the ternary complex compared to the distorted square pyramidal coordination of Cu^{2+}–HSA supports the formation of a copper-mediated complex between HSA and GdL_1.

Molecular Modeling.

Molecular models of the Cu centers in GdL_1, HSA, and the ternary complex were generated on the basis of the coordination geometry and bond lengths for N and O atoms obtained from the EXAFS experimental data (Table 2) using standard MM+ methods. The energy-minimized models are presented in Figure 5. The model of GdL_1–Cu^{2+} reflects a distorted tetragonal geometry around the Cu^{2+} center as predicted by XAS. The geometry of the NTS Cu^{2+} site in HSA reflects a square pyramidal geometry similar to the previously reported crystal structures,[55] while the Cu^{2+} center in the ternary complex is a distorted octahedral geometry. These models support the EPR and XAS data by predicting only small differences in the coordination geometry of GdL_1–Cu^{2+}–HSA compared to that of HSA–Cu^{2+}.

In Vivo Imaging of Free Copper Pools in Living Mice.

Most dietary absorbed copper is transported to the liver via enterohepatic circulation where serum albumin acts as a transporter protein to maintain total exchangeable forms of copper in the μM range.[10,65–70] Hence, the liver plays a key role in copper homeostasis by facilitating copper storage and incorporating copper into ceruloplasmin and other copper

binding proteins. Either elevated or reduced copper in the liver has been associated with neurological disorders and acute liver diseases. Therefore, a noninvasive method to image those abnormalities in copper levels *in vivo* is of broad interest.

To examine whether GdL_1 can detect and respond to changes in extracellular copper *in vivo,* T_1-weighted MR images of C57BL/6 mice were collected at 4.7 T (Figure 6). This imaging field was chosen from the equipment available to us because the r_1 differences between GdL_1 versus GdL_1–Cu–HSA, although smaller at 4.7 T versus 0.47 T (20 MHz), remain significantly different. After i.v. injection of a bolus of 0.1 mmol/kg of GdL_1, the average gain in signal intensity throughout the liver of a healthy mouse was ~25% when compared to the precontrast images. This enhancement returned to baseline after reaching maximum intensity after ~6 min postinjection, reflective of relatively fast excretion of GdL_1 characteristic of most low molecular weight Gd-based extracellular agents. In a separate group, mice were pretreated with the copper chelator, ATN-224 (5 mg/kg), 2 h prior to injection of GdL_1.[38,70] In those animals, the average MR liver enhancement after injection of 0.1 mmol/kg of GdL_1 was lower, ~11% (p-value = 8.6×10^{-3}). This suggests that pretreatment with the copper chelator removed some of the excess Cu^{2+} prior to injection of GdL_1. The tissue distribution of Cu and Gd in the same mice used in the imaging experiments was determined by ICP-MS analysis (Figure 6C). These results confirmed that the higher MR signal intensities directly correlated with higher copper levels in the liver of healthy mice, while the Gd content was identical in both ATN-224 treated and nontreated animals.

Mice were also imaged using two different Gd-based agents as controls, Gadavist (an extracellular agent) and Multihance (a hepatobiliary agent). After injection of an equivalent amount of Gadavist, the signal intensity of liver gained intensity as expected for a typical extracellular agent but only by ~8%. Like GdL_1, the signal gain in liver reached a maximum at ~6 min and then returned to preinjection baseline values at about the same clearance rate as GdL_1. In mice pretreated with ATN-224, the liver enhancement was unchanged, consistent with a lack of affinity of Gadavist for Cu^{2+}. Given that the possibility of a small amount of GdL_1 may clear via hepatobiliary excretion (a complete biodistribution study has not been done), it was important to perform a similar set of control experiments using a known hepatobiliary agent, Multihance, to determine whether ATN-224 treatment might alter liver function. Those imaging results are also presented in Figure 6B. Since the clearance of Multihance in liver was significantly slower than either GdL_1 or Gadavist, the signal intensity data shown here reflect the maximum values at 13 min rather than those at 6 min. As shown, liver image enhancement resulting from the passage of Multihance through the liver was identical in untreated mice versus mice pretreated with ATN-224, showing that liver function is unaltered by ATN-224. Therefore, the decreased intensity we observed when using GdL_1 must reflect a decrease in freely available Cu^{2+} in liver.

3. CONCLUSIONS

In this study, we investigated whether a new macrocyclic gadolinium complex, GdL_1, could act as a Cu^{2+}-responsive MRI contrast agent. We also examined the physical-chemical properties of the ternary GdL_1–Cu^{2+}–HSA complex that resulted in a magnified longitudinal

r_1 relaxivity (20 MHz) of 22.6 mM^{-1} s^{-1}. Our results showed that the observed r_1 enhancement due to the slow tumbling of the ternary complex was sufficient to allow detection of μM levels of freely available Cu^{2+} in the liver by T_1-weighted MR imaging, even at 4.7 T. After injection of GdL_1 into healthy untreated mice, the liver was nicely enhanced at 6 min and image contrast returned to background levels after ~20 min. However, when mice were treated with ATN-224, the MR signal gain in liver images was ~50% less compared to control animals. The lower contrast enhancement observed in the liver of mice pretreated with ATN-224 paralleled the reduction in total liver copper as detected by ICP-MS. On the basis of the ICP results, one can estimate the concentration of GdL_1 in liver at 6 min and ask the question of whether the decreased levels of Cu as detected by ICP-MS are consistent with the imaging results. The total amount of Gd in liver at 6 min was 40 μg/g of wet tissue. If one assumes that GdL_1 remains largely extracellular and that the extracellular fraction of wet liver is ~24–26%,[71,72] then the GdL_1 concentration can be estimated as ~1 mM (40 μg/g divided by 157 g/mol = 0.25 μmol/g = 0.25 μmol/0.26 mL = 1 mM). This same calculation for Cu gives a total [Cu] of 0.36 mM in liver of control mice (6 μg/g) and 0.18 mM in livers after treatment with ATN-224 (3 μg/g). Although not all of the Cu^{2+} is extracellular, a 50% change in available Cu would easily be detected using GdL_1 even if r_1 is no higher than 9 mM^{-1} s^{-1} at 4.7 T. One would expect to see even more dramatic changes in MRI signal intensity in liver if these experiments had been performed at typical clinical imaging fields, 1.5 or 3 T.

The second goal of this study was to identify the Cu^{2+} donor atoms on GdL_1, the donor atoms in the ternary GdL_1–Cu^{2+}–HSA complex, and the location of the GdL_1–Cu^{2+} binding site in HSA. The fact that Cu^{2+} has only one high-affinity site in HSA, the N-terminal site,[55,57] it is reasonable to assume that GdL_1 also binds at this site by contributing donor atoms to Cu^{2+}. This model is consistent with the changes in the Cu^{2+} coordination sphere as reported by EPR and X-ray absorption spectroscopy (XAS) data. The combined results indicate that the Cu^{2+} binds to GdL_1 via a single tertiary N atom and two carboxylate O atoms on GdL_1 and a single water molecule to form a distorted tetragonal complex. The Cu^{2+} center in the GdL_1–Cu^{2+}-HSA ternary complex is most consistent with coordination by four equatorial nitrogen donor atoms from the protein and one or two axial O/N donors from GdL_1, resulting in a distorted octahedral/square pyramidal geometry. The slight coordination changes in the Cu^{2+} center with GdL_1 in the presence of HSA result in a stable ternary complex that results in a surprisingly high r_1 relaxivity at 20 MHz.

In summary, our study shows that GdL_1 can be used as a sensor of excess freely available Cu^{2+} ions in tissue. In the presence of HSA, the freely available Cu^{2+} forms a stable ternary complex GdL_1–Cu^{2+}–HSA that magnifies the r_1 relaxivity to such an extent that *in vivo* detection of exchangeable Cu^{2+} MR imaging was possible. To our knowledge, this is the first time that extracellular copper levels in the liver could be detected and with a remarkable statistical difference. Although this work has not included a mouse disease model to validate the results obtained here, there is enough evidence to suggest that this sensor can be used in mouse models with known abnormal levels of copper. The total serum copper levels can be markedly elevated in acute liver failure due to its release of excess copper ions from liver tissue stores. This results in elevated total serum Cu^{2+} not bound to ceruloplasmin referred to as “free copper”.[73] For example, Wilson’s disease patients reported the significantly

higher concentrations of serum nonceruloplasmin copper (>4.0 μM) in the blood[74] and hepatic copper content of >250 μg/g of dry liver weight.[75,76] Similarly, deficiency of copper has been reported in a variety of genetic, neurological, cardiovascular, and metabolic diseases.[9,77] Furthermore, it has recently been shown that elevated serum and tumor copper levels are linked to the progression of cancer malignancy[78] and also plays an important role in the regulation of sleep-related and arousal behaviors.[79] Therefore, we believe that the observations reported here using GdL_1 will catalyze discoveries of Cu^{2+}-responsive MRI agents for imaging acute liver conditions such as that found in Wilson's diseases or elevated copper levels in other disease conditions.

Supplementary Material

Refer to Web version on PubMed Central for supplementary material.

ACKNOWLEDGMENTS

Financial support from the National Institutes of Health (DK-095416 and EB-015908), the American Diabetes Association (ADA 7-12-IN-42), and the Robert A. Welch Foundation (AT-584 to ADS and AT-1935-20170325 to GM) is gratefully acknowledged. We thank the staff at Beamline 9–3, Stanford Synchrotron Radiation Light Source (SSRL), for support in XAS data collection. We also thank Dr. Alexendar Funk for help with the mouse imaging experiments at UTSW, Drs. Hien Q. Nguyen and Alexios Papadimitrators for their support and training in the ICP-MS, EPR experiments at UT Dallas, and Dr. Limei Zhang at University of Nebraska—Lincoln for discussions on XAS data collection and analysis.

REFERENCES

(1). Puig S; Thiele DJ Molecular mechanisms of copper uptake and distribution. Curr. Opin. Chem. Biol. 2002, 6, 171–180. [PubMed: 12039001]

(2). Maryon EB; Molloy SA; Zimnicka A. m.; Kaplan JH. Copper entry into human cells: progress and unanswered questions. BioMetals 2007, 20, 355–364. [PubMed: 17211679]

(3). Linder MC; Wooten L; Cerveza P; Cotton S; Shulze S; Lomeli N Copper Transport. Am. J. Clin. Nutr. 1998, 67, 965S–971S. [PubMed: 9587137]

(4). Prohaska JR; Gybina AA Intracellular coppert transport in mammals. J. Nutr. 2004, 134, 1003–1006. [PubMed: 15113935]

(5). Lutsenko S; Barnes NL; Bartee MY; Dmitriev OY Function and Regulation of Human Copper-Transporting ATPases. Physiol. Rev. 2007, 87, 1011–1046. [PubMed: 17615395]

(6). Balamurugan K; Schaffner W Copper homeostasis in eukaryotes: teetering on a tightrope. Biochim. Biophys. Acta, Mol. Cell Res. 2006, 1763, 737–746.

(7). Macreadie IG Copper transport and Alzheimer's disease. Eur. Biophys. J. 2008, 37, 295–300. [PubMed: 18004558]

(8). Waggoner DJ; Bartnikas TB; Gitlin JD The role of copper in neurodegenerative disease. Neurobiol. Dis. 1999, 6, 221–230. [PubMed: 10448050]

(9). Que EL; Domaille DW; Chang CJ Metals in neurobiology: probing their chemistry and biology with molecular imaging. Chem. Rev. 2008, 108, 1517–1549. [PubMed: 18426241]

(10). Zatta P; Frank A Copper deficiency and neurological disorders in man and animals. Brain Res. Rev. 2007, 54, 19–33. [PubMed: 17270275]

(11). Bush AI Metals and neuroscience. Curr. Opin. Chem. Biol. 2000, 4, 184–191. [PubMed: 10742195]

(12). Brown DR; Qin K; Herms JW; Madulaung A; Manson J; Strome R; Fraser PE; Kuck T; von Bohlen A; Schulz-Schaeffer W; Giese A; Westway D; Kretzscmar H The cellular prion protein binds copper in vivo. Nature 1997, 390, 684–687. [PubMed: 9414160]

(13). Morgan MT; Bagchi P; Fahrni CJ Fluorescent probes for monovalent copper. Encyclopedia of Inorganic and Bioinorganic. Chemistry. 2004, 1–19.

(14). Rae TD; Schmidt PJ; Pufahl RA; Culotta VC; O'Halloran TV Undetectable intracellular free copper: the requirement of a copper chaperone for superoxide dismutase. Science 1999, 284, 805. [PubMed: 10221913]

(15). Gaggelli E; Kozlowski H; Valensin D; Valensin G Copper homeostasis and neurodegenerative disorders (Alzheimer's, prion, and Parkinson's diseases and amyotrophic lateral sclerosis). Chem. Rev. 2006, 106, 1995–1998. [PubMed: 16771441]

(16). Waggoner DJ; Bartnikas TB; Gitlin JD The role of copper in neurodegenerative disease. Neurobiol. Dis. 1999, 6, 221–230. [PubMed: 10448050]

(17). Desai V; Kaler SG Role of copper in human neurological disorders. Am. J. Clin. Nutr. 2008, 88, 855S–858S. [PubMed: 18779308]

(18). Multhaup G; Schlicksupp A; Hesse L; Beher D; Ruppert T; Masters CL; Beyreuther K The amyloid precursor protein of Alzheimer's disease in the reduction of copper(II) to copper(I). Science 1996, 271, 1406–1409. [PubMed: 8596911]

(19). Bertini I; Rosato A Menkes disease. Cell. Mol. Life Sci. 2008, 65, 89–91. [PubMed: 17989919]

(20). Kaler SG ATP7A-related copper transport diseases-emerging concepts and future trends. Nat. Rev. Neurol. 2011, 7, 15–29. [PubMed: 21221114]

(21). Lutsenko S; Gupta A; Burkhead JL; Zuzel V Cellular multitasking: the dual role of human Cu-ATPases in cofactor delivery and intracellular copper balance. Arch. Biochem. Biophys. 2008, 476, 22–32. [PubMed: 18534184]

(22). Cox D; Moore SD Copper transporting P-type ATPases and human disease. J. Bioenerg. Biomembr. 2002, 34, 333–338. [PubMed: 12539960]

(23). Valentine JS; Doucette PA; Potter SZ Copper-zinc superoxide dismutase and amyotrophic lateral sclerosis. Annu. Rev. Biochem. 2005, 74, 563–593. [PubMed: 15952898]

(24). Peng F; Lutsenko S; Sun X; Musik O Positron emission tomography of copper metabolism in the Atp7b−/− knock-out mouse model of Wilson's disease. Mol. Imaging Biol. 2012, 14, 70–78. [PubMed: 21327972]

(25). Peng F Positron emission tomography for measurement of copper fluxes in live organisms. Ann. N. Y. Acad. Sci. 2014, 1314, 24–31. [PubMed: 24628290]

(26). Aime S; Botta M; Terreno E Gd (III)-based contrast agents for MRI. Adv. Inorg. Chem. 2005, 57, 173–232.

(27). Aime S; Botta M; Fasano M; Terreno E Lanthanide (III) chelates for NMR biomedical applications. Chem. Soc. Rev. 1998, 27, 19–29.

(28). Caravan P; Ellison JJ; McMurry TJ; Lauffer RB Gadolinium(III) Chelates as MRI Contrast Agents: Structure, Dynamics, and Applications. Chem. Rev. 1999, 99, 2293–2352. [PubMed: 11749483]

(29). Moats RA; Fraser SE; Meade TJA 'smart' magnetic resonance imaging agent that reports on specific enzymatic activity. Angew. Chem., Int. Ed. Engl. 1997, 36, 726–732.

(30). Raghunand N; Howison C; Sherry AD; Zhang S; Gillies RJ Renal and Systemic pH Imaging by Contrast-Enhanced MRI. Magn. Reson. Med. 2003, 49, 249–257. [PubMed: 12541244]

(31). Aime S; Botta M; Gianolia E; Terreno E A p(O(2))-Responsive MRI Contrast Agent Based on the Redox Switch of Manganese(II/III) - Porphyrin Complexes. Angew. Chem., Int. Ed. 2000, 39, 747–750.

(32). Berkowitz BA; Wilson CA; Hatchell DL; London RE Quantitative-Determination of the Partial Oxygen-Pressure in the Vitrectomized Rabbit Eye In vivo Using F-19 NMR. Magn. Reson. Med. 1991, 21, 233–241. [PubMed: 1745122]

(33). Que EL; Chang CJ A smart magnetic resonance contrast agent for selective copper sensing. J. Am. Chem. Soc. 2006, 128, 15942. [PubMed: 17165700]

(34). Que EL; Gianolio E; Baker SL; Wong AP; Aime S; Chang CJ Copper-responsive magnetic resonance imaging contrast agents. J. Am. Chem. Soc. 2009, 131, 8527. [PubMed: 19489557]

(35). Li WS; Luo J; Chen ZN A gadolinium(III) complex with 8-amidequinoline based ligand as copper(II) ion responsive contrast agent. Dalton Trans. 2011, 40, 484–492. [PubMed: 21113542]

(36). Jang JH; Bhuniya S; Kang J; Yeom A; Hong KS; Tim JS Cu2+-Responsive Bimodal (Optical/MRI) contrast agent for cellular imaging. Org. Lett. 2013, 15, 4702–4705. [PubMed: 24015763]

(37). Zhang X; Jing X; Liu T; Han G; Li H; Dun C Dual-functional Gadolinium Based Copper (II) probe for selective magnetic resonance Imaging and florescence sensing. Inor. Chem. 2012, 51, 2325–2331.

(38). Hirayama T; Van de Bittner GC; Gray LW; Lutsenko S; Chang CJ Near-infrared fluorescent sensor for in vivo copper imaging in a murine Wilson disease model. Proc. Natl. Acad. Sci. U.S.A. 2012, 109, 2228–2233. [PubMed: 22308360]

(39). Clavijo Jordan MV; Lo S; Chen S; Preihs C; Chirayil S; Zhang S; Kapur P; Li W; Leon-Rodriguez LMD; Lubag AJM; Rofsky NM; Sherry AD Zinc-sensitive MRI contrast agent detects differential release of Zn(II) ions from the healthy vs. malignant mouse prostate. Proc. Natl. Acad. Sci. U.S.A. 2016, 113, E5464–E5471. [PubMed: 27562169]

(40). Lubag AJM; Leon-Rodriguez LMD; Burgess SC; Sherry AD Noninvasive MRI of β-cell function using a Zn^{2+}-responsive contrast agent. Proc. Natl. Acad. Sci. U.S.A. 2011, 108, 18400–18405. [PubMed: 22025712]

(41). Yu J; Martins AF; Preihs C; Clavijo-Jordan V; Chirayil S; Zhao P; Wu Y; Nasr K; Kiefer GE; Sherry AD Amplifying the sensitivity of Zinc(II) responsive MRI contrast agents by altering water exchange rates. J. Am. Chem. Soc. 2015, 137, 14173–14179. [PubMed: 26462412]

(42). Esqueda AC; López JA; Andreu-de-Riquer G; Alvarado-Monzón JC; Ratnakar J; Lubag AJM; Sherry AD; De León-Rodríguez LM A new gadolinium-based MRI zinc sensor. J. Am. Chem. Soc. 2009, 131, 11387–11391. [PubMed: 19630391]

(43). Gaur A; Klysubun W; Nair NN; Shrivastava BD; Prasad J; Srivatava K XAFS study of copper(II) complexes with square planar and square pyramidal coordination geometries. J. Mol. Struct. 2016, 1118, 212–218.

(44). Laussac JP; Sarkar B Characterization of the copper(II)- and nickel(II)-transport site of human serum albumin. Studies of copper(II) and nickel(II) binding to peptide 1–24 of human serum albumin by 13C and 1H NMR spectroscopy. Biochemistry 1984, 23, 2832–2838. [PubMed: 6547847]

(45). Zgirski A; Frieden E Binding of Cu(II) to non-prosthetic sites in ceruloplasmin and bovine serum albumin. J. Inorg. Biochem. 1990, 39, 137–148. [PubMed: 2380706]

(46). Bal W; Christodoulou J; Sadler PJ; Tucar A Multi-metal binding site of serum albumin. J. Inorg. Biochem. 1998, 70, 33–39. [PubMed: 9661286]

(47). Lu J; Stewart AJ; Sadler PJ; Pinheiro TJT; Blindauer CA Albumin as a zinc carrier: properties of its high-affinity zincbinding site. Biochem. Soc. Trans. 2008, 36, 1317–1321. [PubMed: 19021548]

(48). Shakdofa M; Shtaiwi M; Morsy N; Abdel-raseel TMA Metal complexes of hydrazones and their biological, analytical and catalytic applications: A review. Main Group Chem. 2014, 13, 187–218.

(49). Zhan G; Zhong W; Wei Z; Liu Z; Liu X Roles of phenol groups and auxiliary ligand of copper(ii) complexes with tetradentate ligands in the aerobic oxidation of benzyl alcohol. Dalton Transactions 2017, 46, 8286–8297. [PubMed: 28621375]

(50). Vymazal J; Bulte JWM; Frank JA; Chiro GD; Brooks RA Frequency dependence of MR relaxation times I. Paramagnetic ions. J. Magn. Reson. Imaging 1993, 3, 637–640. [PubMed: 8347957]

(51). Casella L; Gullotti M; Pallanza G; Pinter A; Marchesini A Spectroscopic and binding studies of azide to type-2-copper-depleted ascorbate oxidase from zucchini. Biol. Metals. 1991, 4, 81–89.

(52). Job P Formation and Stability of Inorganic Complexes in Solution. Ann. Chim. (Paris) 1928, 113–115.

(53). Guo M; Zou J; Li P; Shang Z; Hu G; Yu Q Binding interaction of gatifloxacin with bovine serum albumin. Anal. Sci. 2004, 20, 465–470. [PubMed: 15068289]

(54). Cabaniss SE; Shuman MS Combined ion selective electrode and fluorescence quenching detection for copper-dissolved organic matter titrations. Anal. Chem. 1986, 58, 398–401.

(55). Hureau C; Eury H; Guillot R; Bijani C; Sagen S; Solari P; Guillon E; Faller P; Dorlet P X-ray and Solution Structures of Cu^{II}GHK and Cu^{II}DAHK Complexes: Influence on Their Redox Properties. Chem.—Eur. J. 2011, 17, 10151–10160. [PubMed: 21780203]

(56). Bal W; Christodoulou J; Sadler PJ; Tucker A Multi-metal binding site of serum albumin. J. Inorg. Biochem. 1998, 70, 33–39. [PubMed: 9661286]

(57). Rozga M; Sokolowska M; Protas AM; Bal W Human serum albumin coordinates Cu(II) at its N-terminating binding site with 1pM affinity. JBIC, J. Biol. Inorg. Chem. 2007, 12, 913–918. [PubMed: 17516096]

(58). Bal W; Sokołowska M; Kurowska E; Faller P Binding of transition metal ions to albumin: Sites, affinities and rates. Biochim. Biophys. Acta, Gen. Subj. 2013, 1830, 5444–5455.

(59). Neumann PZ; Sass- Kortsark A The state of copper in human serum: evidence for an amino acid-bound fraction. J. Clin. Invest. 1967, 46, 646–658. [PubMed: 6021211]

(60). Tweedle MF; Hagan JJ; Kumar K; Mantha S; Chang CA Reaction of gadolinium chelates with endogenously available ions. Magn. Reson. Imaging 1991, 9, 409–415. [PubMed: 1881260]

(61). Xiao Y.-m; Zhao G; Fang X; Zhao Y; Wang G; Yang W; Xu JA smart copper(II)-responsive binuclear gadolinium(III) complex-based magnetic resonance imaging contrast agent. RSC Adv. 2014, 4, 34421–34427.

(62). Sadler PJ; Viles JH 1H and (113)Cd NMR Investigations of Cd(2+) and Zn(2+) Binding Sites on Serum Albumin: Competition with Ca(2+), Ni(2+), Cu(2+), and Zn(2+). Inorg. Chem. 1996, 35, 4490–4496. [PubMed: 11666670]

(63). Martins DA; Gourea LR; Muniz GS; Louro S; Gama D; Soeiro M; Teixeira LR Norfloxacin and N-Donor Mixed-Ligand Copper(II) Complexes: Synthesis, Albumin Interaction, and Anti-Trypanosoma cruzi Activity. Bioinorganic chemistry and application 2016, 2016, 1–11.

(64). Sano M; Komorita S; Yamatera H XANES spectra of copper(II) complexes: correlation of the intensity of the 1s.fwdarw. 3d transition and the shape of the complex. Inorg. Chem. 1992, 31, 459–463.

(65). Askwith C; Eide D; Van Ho A; Bernard PS; Li L; Davis-Kaplan S; Sipe DM; Kaplan J The FET3 gene of S. cerevisiae encodes a multicopper oxidase required for ferrous iron uptake. Cell 1994, 76, 403–10. [PubMed: 8293473]

(66). Linder MC, Massaro EJ, Eds. Handbook of copper pharmacology and toxicology; Humana Press: Totowa, NJ, 2002; pp 3–32.

(67). Vural H; Uzun K; Uz E; Kocgigil A; Cigli A; Akyol O Concentration of copper, zinc and various elements in serum of patients with bronchial asthma. J. Trace Elem. Med. Biol. 2000, 14, 88–91. [PubMed: 10941719]

(68). Alebic-Juretic A; Frkovic A Plasma copper concentrations in pathological pregnancies. J. Trace Elem. Med. Biol. 2005, 19, 191–194. [PubMed: 16325535]

(69). Linder MC; Wooten L; Cerveza P; Cotton S; Shulze S; Lomeli N Copper transport. Am. J. Clin. Nutr. 1998, 67, 965S–971S. [PubMed: 9587137]

(70). Lowndes SA; Sheldon HV; Cai S; Taylor JM; Harris AL Copper chelator ATN-224 inhibits endothelial function by multiple mechanisms. Microvasc. Res. 2009, 77, 314–326. [PubMed: 19323979]

(71). Barratt TM; Walser M Extracellular fluid in individual tissues and in whole animals: the distribution of radiosulfate and radiobromide. J. Clin. Invest. 1969, 48, 56–66. [PubMed: 5765027]

(72). Guo SL; Su LN; Zhai YN; Chirume WM; Lei JQ; Zhang H; Yang L; Shen XP; Wen XX; Guo YM The clinical value of hepatic extracellular volume fraction using routine multi phasic contrast-enhanced liver Ct for staging liver fibrosis. Clin. Radiol. 2017, 72, 242–246. [PubMed: 28341030]

(73). Ferenci P; Czlonkowska A; Merle U; Ferenc S; Gromadzka G; Yurdaydin C; Vogel W; Bruha R; Schmidt HT; Strmmel W Late-onset Wilson's disease. Gastroenterology 2007, 132, 1294–1298. [PubMed: 17433323]

(74). Frommer DJ Direct measurement of serum non-caeruloplasmin copper in liver disease. Clin. Chim. Acta 1976, 68, 303–307. [PubMed: 1277546]

(75). Yang X; Tang XP; Zhang YH; Luo KZ; Jiang YF; Luo HY; Lei JH; Wang WL; Li MM; Chen HC; Deng SL; Lai LY; Liang J; Zhang M; Tian Y; Xu Y Prospective evaluation of the diagnostic accuracy of hepatic copper content, as determined using the entire core of a liver biopsy sample. Hepatology 2015, 62, 1731–41. [PubMed: 26095812]

(76). Poujois A; Trocello J-M; Djebrani-Oussedik N; Poupon J; Collet C; Girardot-Tinant N; Sobesky R; Habès D; Debray D; Vanlemmens C; Fluchère F; Ory-Magne F; Labreuche J; Preda C; Woimant F Exchangeable copper: a reflection of the neurological severity in Wilson's disease. European Journal of Neurology. 2017, 24, 154–160. [PubMed: 27739240]

(77). Heffern MC; Park HM; Au-Yeung HY; Van de Bittner GC; Ackerman CM; Stahl A; Chang CJ In vivo bioluminescence imaging reveals copper deficiency in a murine model of nonalcoholic fatty liver disease. Proc. Natl. Acad. Sci. U. S. A. 2016, 113, 14219–14224. [PubMed: 27911810]

(78). Mumper RJ; Gupte A Elevated copper and oxidative stress in cancer cells as a target for cancer treatment. Cancer Treat. Rev. 2009, 35, 32–46. [PubMed: 18774652]

(79). Xiao T; Ackerman CM; Carroll EC; Jia S; Hogland A; Chan J; Thai B; Liu CS; Iscacoff EY; Chang CJ Copper regulates rest-activity cycles through the locus coeruleus-norepinephrine system. Nat. Chem. Biol. 2018, 14, 655–663. [PubMed: 29867144]

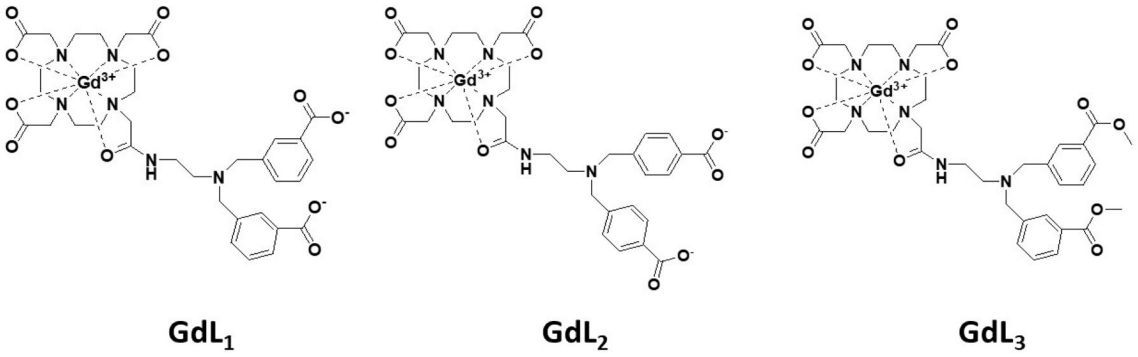

Figure 1.
Gadolinium-DO3A-based copper responsive (GdL) agents.

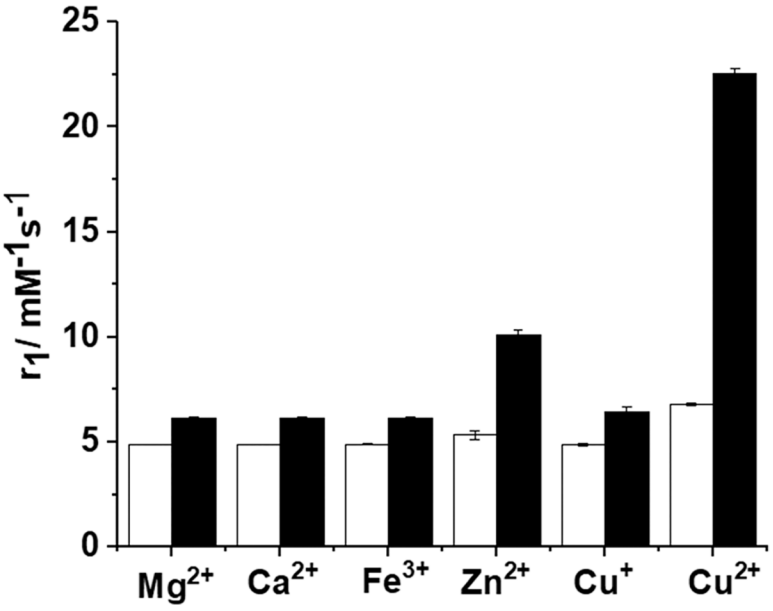

Figure 2.

20 MHz relaxivity (r_1) of GdL_1 in the presence of various M^{n+} ± HSA. The white bars reflect r_1 after addition of 0.5 mM Mg^{2+}, Ca^{2+}, Fe^{3+}, Zn^{2+}, Cu^{+}, or Cu^{2+} to 0.5 mM solutions of GdL_1. The black bars reflect r_1 after subsequent addition of 0.6 mM HSA to the GdL_1–M^{n+} solutions. The data were collected in 0.1 M MOPS buffer (pH 7.4) at 37 °C.

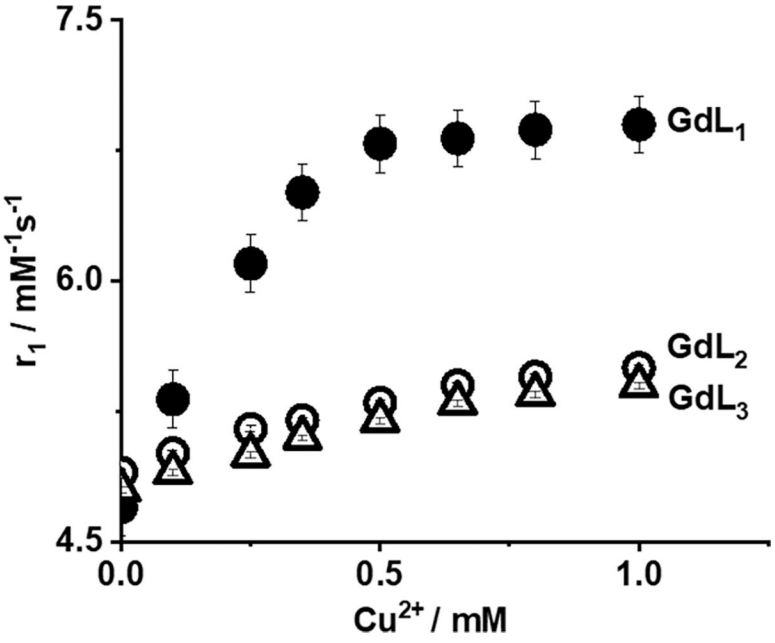

Figure 3.

20 MHz r_1 relaxivity of $GdL_{1–3}$ as a function of added Cu^{2+}. The concentration of $GdL_{1–3}$ was 0.5 mM in 0.1 M MOPS buffer (pH 7.4). The data were collected at 37 °C.

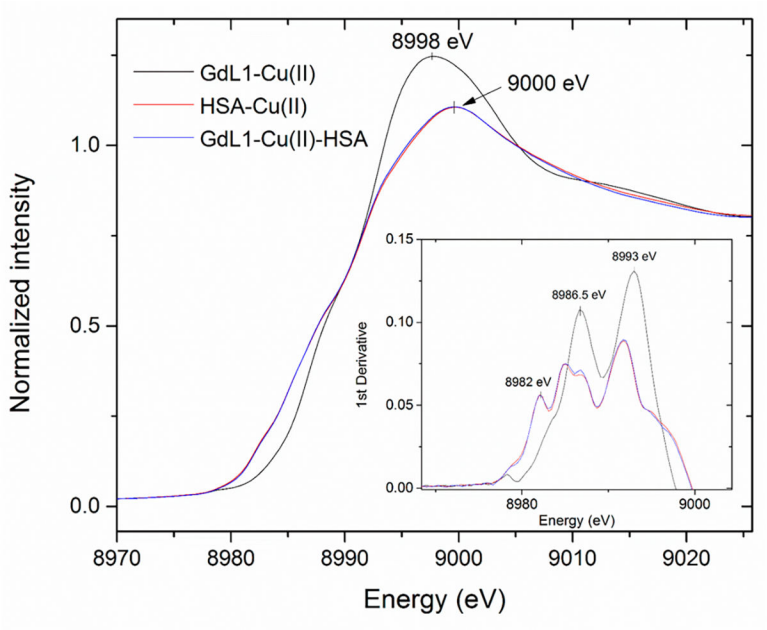

Figure 4.
XANES spectra for GdL_1 in the presence of Cu^{2+} and HSA.

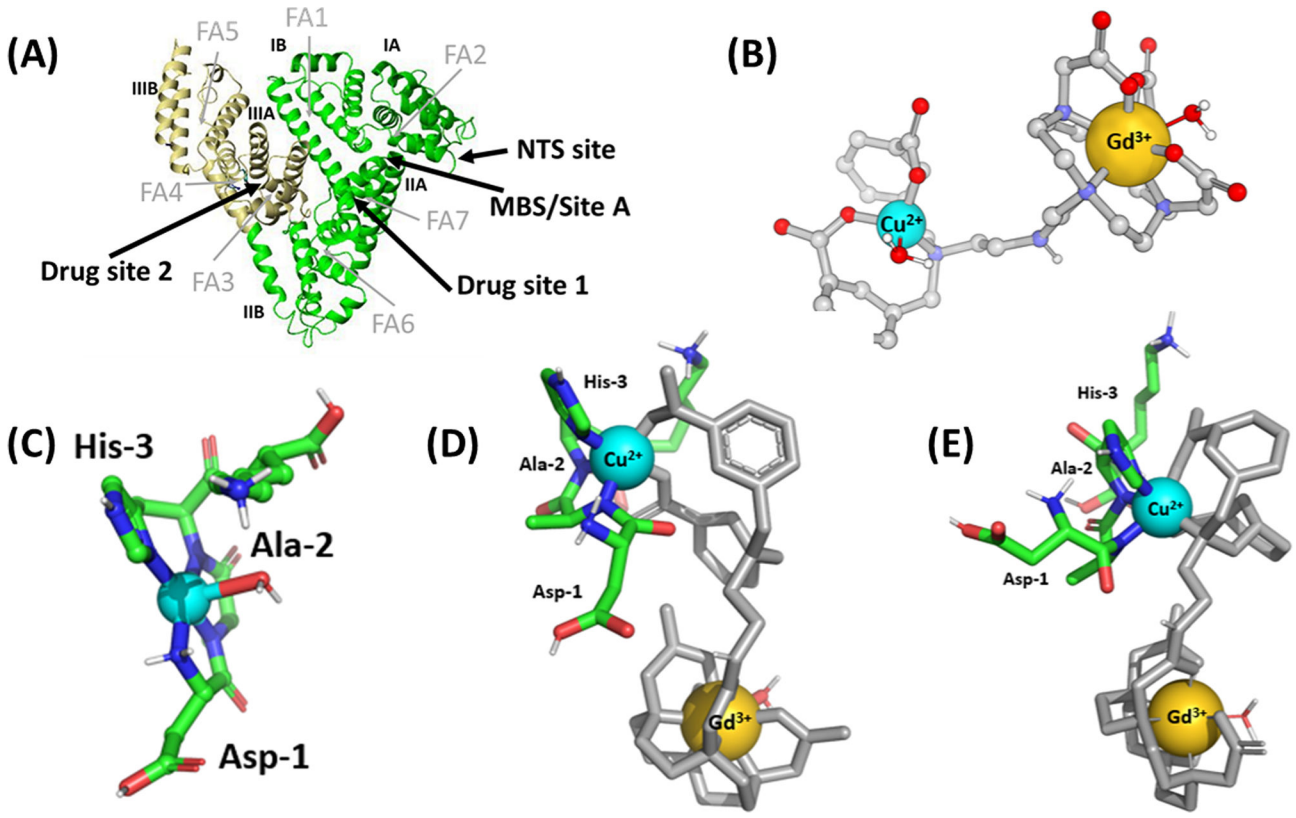

Figure 5.

MM+ minimized structures of (A) the domain structure of albumin (PDB ID code 1AO6): domains I and II are colored green (residues 1–373), and domain III is colored in yellow (residues 380–571); long chain fatty acid sites (FA), Sudlow's drug binding sites, Cu^{2+} binding NTS site, and zinc binding site A (MBS/site A) are also shown. (B) GdL_1–Cu^{2+} complex. (C) HSA–Cu^{2+} complex (CCDC-809109).[52] (D) HSA–Cu^{2+}–GdL_1 distorted square pyramidal complex. (E) HSA–Cu^{2+}–GdL_1 distorted octahedral complex consistent with all NMR, XAS, and EXAFS data. Hydrogen atoms and other sites of HSA have been removed to simplify visualization. Only residues at the NTS site in HSA are included. These figures were generated using Hyperchem7.5.

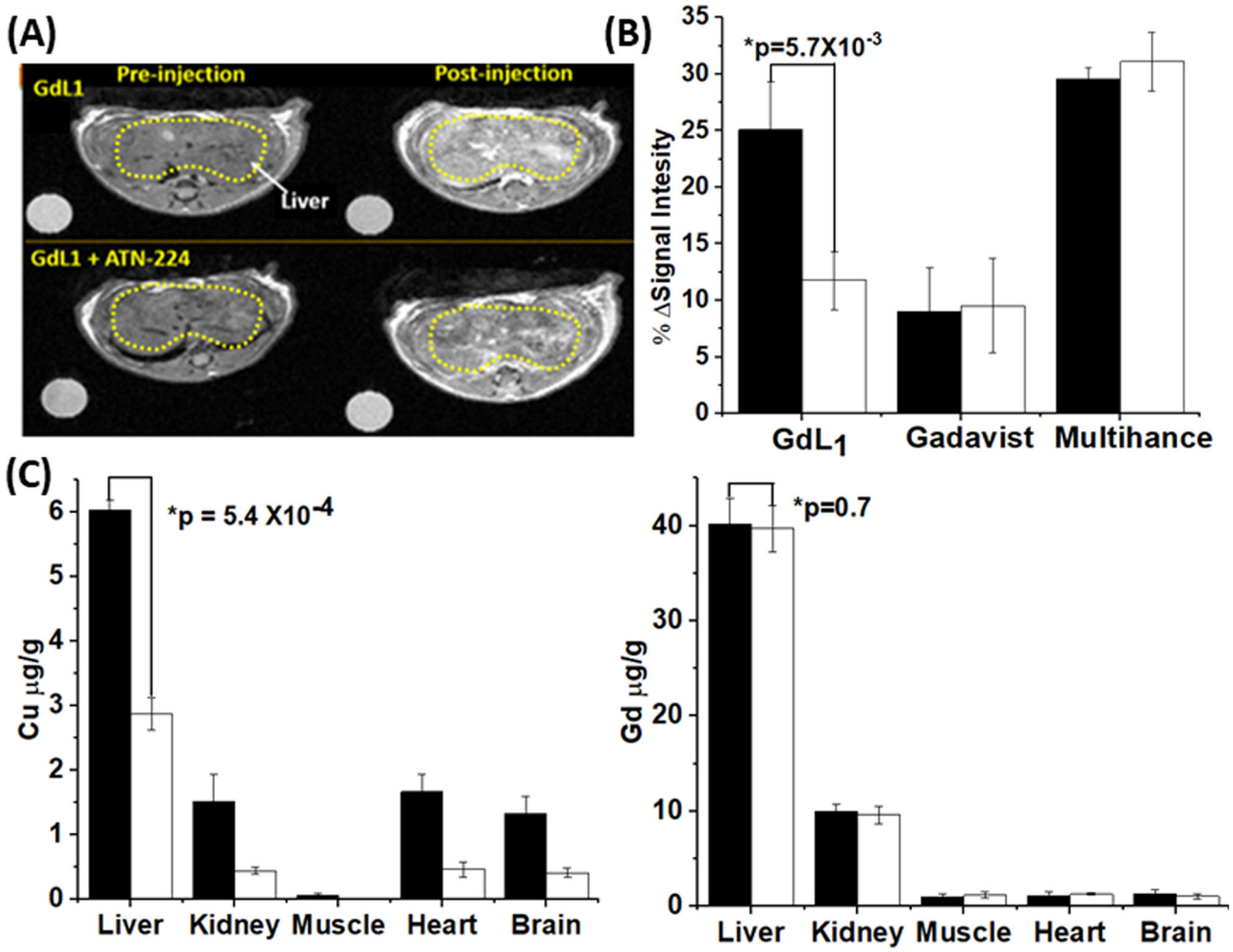

Figure 6.

(A) *In vivo* MRI images of wild type mouse ($n = 3$) pre- and postinjection of GdL_1 (0.1 mmol/kg) without (top) or with (bottom) pretreatment with ATN-224 (5 mg/kg in 50 μL). All images were obtained at 4.7 T. (B) The average MRI signal intensity of mouse liver 6 min after injection of either GdL_1 or Gadavist in control mice (black bars) versus mice pretreated with ATN-224 (white bars). The columns on the right show average liver signal intensities at 13 min after injection with Multihance. The data were compared using a two-tailed student *t* test. $*p < 0.05$ ($n = 3$); error bars reflect ± SD. (C) Total Cu and Gd (μg/g of tissue) in various tissues collected from control mice (black bars) and from mice pretreated with ATN-224 (white bars) 6 min after the injection of GdL_1. Tissue copper levels relative to tissue wet weight were determined by ICP-MS. The data were compared using a two-tailed student *t* test. $*p < 0.05$ ($n = 3$); error bars reflect ± SD.

Table 1.

20 MHz Relaxivity Values for $GdL_{1–3}$ ± Cu^{2+} and ± HSA and K_d Values for Binding of $GdL_{1–3}$–Cu^{2+} with HSA[a]

	in the absence of 0.6 mM HSA				in the presence of 0.6 mM HSA			
	r_1 (mM^{-1} s^{-1})				r_1 (mM^{-1} s^{-1})			
GdLx	**no Cu^{2+}**	**1 equiv of Cu^{2+}***	**% increase in r_1**	**K_d (GdL–Cu^{2+})[b] (μM)**	**no Cu^{2+}**	**1 equiv of Cu^{2+}**	**% increase in r_1**	**K_d (GdL–Cu^{2+}–HSA)[c] (μM)**
GdL_1	4.7 ± 0.1	6.7 ± 0.1	43%	84 ± 10	6.1 ± 0.1 5.7 ± 0.1[d]	22.6 ± 0.2 15.4 ± 0.2[d]	270%	45 ± 3.1
GdL_2	4.9 ± 0.2	5.5 ± 0.1	12%	895 ± 32	6.5 ± 0.2	14.5 ± 0.1	123%	59 ± 5
GdL_3	4.8 ± 0.1	5.4 ± 0.2	12%	352 ± 9	6.3 ± 0.2	12.0 ± 0.2	90%	60 ± 10

[a] All experiments were performed in 0.1 M MOPS buffer (pH 7.4) at 37 °C.

[b] $K_{d(GdL–Cu^{2+})}$ was determined by fluorescence titrations.

[c] $K_{d(GdL–Cu^{2+}–HSA)}$ was determined by proton relaxation enhancement titrations.

[d] Values measured in the presence of 0.6 mM mouse albumin.

Table 2.

Structural and Coordination Parameters Obtained from Fitting Cu K-edge EXAFS[a]

complex	*N*	bond	*R* (Å)	σ^2 (Å^2)	*F*-factor
GdL_1–Cu(II)	3	Cu–N/O	1.994(3)	0.0008	0.488
	1	Cu–N/O	2.51(1)	0.0001	
Cu(II)–HSA	3	Cu–N/O	1.991(2)	0.0016	0.398
	1	Cu–N/O	2.278(7)	0.0013	
	1	Cu–N/O	2.515(7)	0.0008	
GdL_1–Cu(II)–HSA	3	Cu–N/O	1.954(6)	0.0054	0.576
	1	Cu–N/O	2.33(1)	0.0037	
	1	Cu–N/O	2.86(1)	0.0001	
GdL_1–Cu(II)–HSA	4	Cu–N/O	1.965(6)	0.0054	0.587
	1	Cu–N/O	2.31(2)	0.0037	
	1	Cu–N/O	2.87(1)	0.0001	

[a]Coordination numbers are indicated by *N*, interatomic distances *R* are given in Å (the values in parentheses are the estimated standard deviations), Debye–Waller factors σ^2 (the mean-square deviations in interatomic distance) are given in Å^2, and the fit-error function *F* is defined $K_{\mathrm{d}}\left(\mathrm{GdL}-\mathrm{Cu}^{2+}-\mathrm{HSA}\right)$, where $\chi^{(\mathrm{k})}$ are the EXAFS oscillations and *k* is the photoelectron wave-number.